PNAS

Supplementary Information for

A sequential two-step priming scheme reproduces diversity in synaptic strength and short-term plasticity

Kun-Han Lin[1,$], Holger Taschenberger[2,$,*], and Erwin Neher[1,3,*]

[1]Emeritus Laboratory of Membrane Biophysics, Max Planck Institute for Multidisciplinary Sciences, Göttingen, Germany

[2]Department of Molecular Neurobiology, Max Planck Institute for Multidisciplinary Sciences, Göttingen, Germany

[3]Cluster of Excellence "Multiscale Bioimaging", Georg August University, Göttingen, Germany

[$] these authors contributed equally

[*] Correspondence: eneher@mpinat.mpg.de, taschenberger@mpinat.mpg.de

This PDF file includes:

Material and Methods

Animal Maintenance

Juvenile, post-hearing onset (P14–16) Wistar rats of either sex were used. All experiments complied with the German Protection of Animals Act and with the guidelines for the welfare of experimental animals issued by the European Communities Council Directive. Animal health was controlled daily by caretakers. Animals were kept at 21 ± 1°C and 55% relative humidity with a 12 h/12 h light/dark cycle. Food and tap water were provided ad libitum, and cages were changed at least once a week.

Slice Preparation

Acute brainstem slices were prepared similarly as previously described (1). After decapitation, brains were dissected out quickly and immersed in ice-cold carbogenated (95% O_2, 5% CO_2) low-Ca^{2+} low-Na^+ artificial CSF (aCSF) containing (in mM): 93 NMDG, 2.5 KCl, 0.5 $CaCl_2$, 25 glucose, 10 $MgCl_2$, 20 HEPES, 1.25 NaH_2PO_4, 30 $NaHCO_3$, 2 thiourea, 5 sodium ascorbate, 3 Na-pyruvate, pH 7.4 with HCl (2, 3). The brainstem was glued onto the stage of a VT1000S vibratome (Leica), and 200 µm-thick coronal slices containing the medial nucleus of the trapezoid body (MNTB) were cut. Slices were incubated for 40 min at 35°C in a chamber containing normal aCSF containing (in mM): 125 NaCl, 2.5 KCl, 2 $CaCl_2$, 1 $MgCl_2$, 25 glucose, 25 $NaHCO_3$, 1.25 NaH_2PO_4, 0.4 ascorbic acid, 3 myoinositol, and 2 Na-pyruvate (pH 7.4, bubbled with 95% O_2, 5% CO_2). Slices were kept at room temperature (21–24°C) and used for recordings for up to 4 h after recovery.

Electrophysiology

Whole-cell patch-clamp recordings were made from principal neurons (PNs) of the MNTB at room temperature using an EPC-10 amplifier controlled by PatchMaster software (HEKA Elektronik). Patch-pipettes pulled from borosilicate glass (Science Products) were coated with dental wax in order to reduce stray capacitance. They had an open-tip resistance of 2.5–3.5 MΩ when filled with a Cs-gluconate based solution containing (in mM): 100 Cs-gluconate, 30 TEA-Cl, 30 CsCl, 10 HEPES, 5 EGTA, 5 Na_2-phosphocreatine, 4 ATP-Mg, 0.3 GTP, pH 7.2 with CsOH. During experiments, slices were continuously perfused with normal aCSF solution containing 1 mM $MgCl_2$ and 2 mM $CaCl_2$ and supplemented with 5 µM strychnine, to block glycinergic IPSCs. Cells were visualized by using infrared light and oblique illumination (Dodt gradient contrast) through a 60× water-immersion objective (NA = 1.0, Olympus) using an upright BX51WI microscope (Olympus).

All experiments were performed at room temperature. A bipolar stimulation electrode was used to evoke presynaptic APs (stimulus intensity ≤20 V, 100 µs duration). Series resistance (R_s) was ≤8 MΩ and compensated ≥82%. Holding potential (V_h) and leak current were −70 mV and ≤300 pA, respectively. Sampling interval and low-pass filter settings were 20 µs and 5.0 kHz, respectively. To reduce eEPSC amplitudes for improved voltage-clamp and in order to attenuate postsynaptic AMPAR saturation and AMPAR desensitization, all experiments were performed in the continuous presence of 1 mM of the low-affinity GluR antagonist kynurenic acid (kyn) (4-6). The blocking ratio $eEPSC_{kyn}$ / $eEPSC_{ctrl}$ was measured for

a subset of synapses and amounted to 0.127 ± 0.005. Voltage-clamp errors caused by remaining uncompensated R_s were corrected off-line and fully compensated by applying a software correction procedure similar to that described in (7). All offline analysis of electrophysiological data and all numerical simulations were performed using Igor Pro (Wavemetrics). Differential equations were solved numerically using the fifth-order Runge-Kutta-Fehlberg algorithm implemented in Igor Pro. Original data are presented as mean ±SEM.

Decomposition of quantal release into distinct components using non-negative tensor factorization

Non-negative tensor factorization (NTF) of eEPSC trains was performed similarly as previously described (8): In a total of 35 P14–16 post-hearing calyx of Held synapses, eEPSC trains evoked by afferent-fiber stimulation using trains consisting of 40 stimuli delivered at stimulation frequencies (f_{stim}) of 0.5, 1, 2, 5, 10, 20, 50, 100 and 200 Hz were recorded. For NTF, however, only data within the frequency range 5–200 Hz were used. To convert eEPSC peaks into quantal content (m), we assumed an effective quantal size $q^* = -6.6$ pA in the presence of 1 mM kyn in the bath (8, 9). At least three eEPSC train repetitions were analyzed for each stimulus frequency and the respective m_j values for each stimulus j were averaged. For the 35 synapses analyzed here, the NTF data set therefore consisted of 35 × 40 data matrices, one matrix for each of the six f_{stim}. NTF data were thus standard tensors consisting of one layer, except for the two highest f_{stim}: For 100 and 200 Hz stimulation, two additional tensor layers were obtained by pre-conditioning the synapses with either 2 or 4 stimuli delivered at a frequency of 10 Hz. During data acquisition, synapses were allowed to rest after each stimulus train to completely recover from activity-induced changes in synaptic transmission back to resting conditions (15 s following ≤10 Hz trains, 25 s following 20 and 50 Hz, 40 s following 100 and 200 Hz). The order of the stimulus trains was pseudo-randomized for each synapse to avoid a contamination of the data with systematic run-down or run-up trends. The total time of a recording session to gather all NTF data from a single calyx synapse was ~21 min.

NTF analysis was performed in two sequential steps: (1) In a first step, a two-component NTF was performed to obtain the two basefunctions (BFs) BF_{TS} and $BF_{LS,RS}$, which represent release contributed by those SVs that were already in a tightly docked state (SV_{TS}s) prior to stimulation and of those that were not ($SV_{LS,RS}$s), respectively. Both BFs were initialized as previously described (8) and 200 iterations were used during which the goodness of fit was tracked. (2) In a subsequent step, a three-component NTF decomposition was performed providing three basefunctions BF_{TS}, BF_{LS} and BF_{RS} representing release of those SV that were either in a tightly (SV_{TS}s) or a loosely (SV_{LS}s) docked state prior to stimulation and those SVs which were in neither of these two states (SV_{RS}s), respectively. During this second step of analysis, the time course of BF_{TS} was constrained to the result of the previous two-component NTF decomposition, and only 100 iterations were used.

The three-component NTF analysis was performed similarly as described earlier (8) with the following two modifications: (1) The estimate for the mean M_{LS} was biased during iterations by shifting it at each cycle by 35% towards a pre-determined target value. This is necessary, because three-component NTF

analysis does not ensure a unique separation between M_{LS} and M_{RS} (8). The target value was calculated the following way: Assuming that the fast releasing pool of SVs (*FRP*), as calculated by standard methods (Fig. 2C), constitutes the sum of the two components M_{TS} + M_{LS}, we subtracted the mean M_{TS} from the *FRP* to obtain an estimate for M_{LS}, which – provided all preexisting SV_{LS}s are consumed during the trains – equals $SP_{LS,rest}$. However, this estimate needs further correction, since the *FRP* is not completely depleted even at 200 Hz stimulation. Therefore, we determined this estimate, *FRP'*, for 3 frequencies (50, 100 and 200 Hz) and plotted 1 / *FRP'* vs. inter-stimulus interval (ISI). By extrapolating a regression line of this plot to ISI = 0 ms, we effectively obtain an *FRP* estimate for infinite stimulation frequency (f_{stim}) and assume that this approach compensates for incomplete *FRP* depletion (inset Fig. 2C) (10, 11). (2) We introduced an additional constraint on the parameter s_2. Again, the requirement for such a constraint derives from the fact, that NTF decomposition is compatible with a multitude of solutions, and constraints are necessary to arrive at solutions of interest. The standard NTF algorithm (8) already includes a number of general constraints, such as the requirement that m_1 should be very similar for all f_{stim}. Eq. **25**, below, can be solved for s_2, which we used as a constraint, which is specific for the sequential model at f_{stim} = 5–20 Hz. For implementing this constraint, we fitted after each iteration a model curve for BF_{LS} to the mean BF_{LS} for 5–20 Hz stimulation. This fit returns an estimate for s_2 (see below). Deviations between the fitted s_2 and its value according to Eq. **25** were corrected for by compressing or expanding the time course of BF_{LS} in analogy to the p_{fusion} correction described in Neher and Taschenberger (8).

General assumptions underlying the kinetic scheme of SV priming and fusion

For the formulation of the kinetic SV priming and fusion scheme (Fig. 1) we consider a simple sequence of steps in the buildup of a mature fusion-competent release machinery, which implies the following five main features: (1) Docking and priming of SVs occurs at a single type and a fixed number of release sites. (2) SV docking and priming steps are reversible and in dynamic equilibrium with each other at rest. (3) At rest, release sites can be either empty or occupied by an SV residing in one of two states of functional maturation of its release machinery (referred to as SV_{LS} and SV_{TS}). (4) Only SVs equipped with a mature release machinery (SV_{TS}s) are fusion-competent. (5) The priming rate constants k_1 and k_2 are Ca^{2+}-dependent, while the unpriming rate constants b_1 and b_2 have fixed values.

A simple sequential kinetic scheme reproduces experimentally observed STP for frequencies up to 20 Hz

To model the time course of synchronous AP-triggered transmitter release and the temporal pattern of STP at calyx synapses in the frequency range 1 to 20 Hz we use a kinetic scheme as shown in Fig. 1B1. We assume a fixed number of functionally identical release sites (N_{tot}), which at a given time t can either be empty (N_e) or occupied with a docked and primed SV. After the translocation to a release site, docking and priming of a SVs proceeds by transition through two sequential maturation states: Newly arriving SVs are initially loosely docked (SV_{LS}) before they mature into a tightly docked fusion competent SV (SV_{TS}). Thus, the entire pool of

docked and primed SVs at a given time *t* can be subdivided into a subpool of SV_{LS}s (SP_{LS}) and a subpool of SV_{TS}s (SP_{TS}), such that

$$N_{tot} = N_e(t) + SP_{LS}(t) + SP_{TS}(t) \quad (1)$$

Given the kinetic scheme illustrated in Fig. 1B, the following coupled differential equations describe temporal changes in $SP_{LS}(t)$ and $SP_{TS}(t)$ after elimination of $N_e(t)$:

$$\frac{d}{dt} SP_{LS}(t) = -(b_1 + k_1 + k_2) \cdot SP_{LS}(t) + (b_2 - k_1) \cdot SP_{TS}(t) + k_1 \cdot N_{tot} \quad (2)$$

$$\frac{d}{dt} SP_{TS}(t) = k_2 \cdot SP_{LS}(t) - b_2 \cdot SP_{TS}(t) \quad (3)$$

Here the two backward (unpriming) rate constant b_1 and b_2 have fixed values, and the two forward (priming) rate constants k_1 and k_2 are modeled as Ca^{2+}-dependent quantities which increase linearly with $[Ca^{2+}]$, according to:

$$k_1(t) = k_{1,rest} + \sigma_1 \cdot ([Ca^{2+}](t) - [Ca^{2+}]_{rest}) \quad (4)$$

$$k_2(t) = k_{2,rest} + \sigma_2 \cdot ([Ca^{2+}](t) - [Ca^{2+}]_{rest}). \quad (5)$$

$[Ca^{2+}]_{rest}$ represents the resting $[Ca^{2+}]$, which was assumed to be 50 nM (12). σ_1 and σ_2 are linear slope factors characterizing the Ca^{2+}-dependence of the SV priming steps.

The differential equations were solved numerically between APs, together with those for variables *y* and *z* (see Eqs. **40**, **41** below) and a rate equation for $[Ca^{2+}](t)$, which was assumed to decay back to its resting value $[Ca^{2+}]_{rest}$ with a rate constant k_{Ca}:

$$\frac{d}{dt} [Ca^{2+}](t) = -k_{Ca} \cdot ([Ca^{2+}](t) - [Ca^{2+}]_{rest}) \quad (6)$$

For each release event, the quantal content m_j of the $eEPSC_j$ triggered by stimulus *j* was calculated as the product of $p_{fusion,j} \cdot SP_{TS}(t_j)$ with both quantities evaluated immediately before stimulus arrival. Indices such as *j*, as well as *ss* and 1 are used here and in the following to indicate stimulus index, *j* =1 to 40, steady state and first stimulus, respectively. SP_{TS} was decremented by m_j and the number of empty sites were incremented by the same amount. $[Ca^{2+}]$ was incremented by $\Delta[Ca^{2+}] \cdot y(t)$.

To calculate $p_{fusion,j}$, we used an empirical model which requires integration of two variables *y* and *z*, representing facilitation and a small decline in $p_{fusion,j}$ during trains, respectively, as indicated by NTF analysis (see below). Equations 4 and 5 together with Eqs. **1**–**3** provide the following analytical expressions for resting values $N_{e,rest}$, $SP_{LS,rest}$ and $SP_{TS,rest}$ at $t = 0$:

$$N_{e,rest} = N_{tot}/\left(1 + k_{1,rest}/b_1 \cdot \left(1 + k_{2,rest}/b_2\right)\right) \quad (7)$$

$$SP_{LS,rest} = N_{e,rest} \cdot k_{1,rest}/b_1 \quad (8)$$

$$SP_{TS,rest} = SP_{LS,rest} \cdot k_{2,rest}/b_2 \quad (9)$$

where $k_{1,rest}$ and $k_{2,rest}$ according to Eqs. **4** and **5** are the resting values of the forward rate constants k_1 and k_2 evaluated at $[Ca^{2+}] = [Ca^{2+}]_{rest}$.

This simple kinetic scheme of SV priming and fusion described so far reproduces quite well the experimentally observed time courses of synchronous AP-evoked release at calyx synapses for stimulus frequencies ≤20 Hz. For f_{stim} ≥50 Hz, however, extensions to this scheme had to be made in order to fit experimental data without systematic deviations. These extensions (Fig. 1C) are explained in detail in in the Results section.

Derivation of initial guesses and constraints for model parameters from steady-state conditions

Although the simple kinetic scheme presented above only describes STP in response to f_{stim} ≤20 Hz, it is nevertheless instrumental in deriving steady-state values and initial guesses for several model parameters from approximate analytical solutions. Considering that measured release time courses and NTF-derived BFs for stimulus frequencies between 5 to 20 Hz are very similar when plotted versus stimulus number *j* (Fig. 3A), it is convenient to formulate Eqs. **2**–**5** in terms of the ISI as the unit of time and integrating Eqs. **5** and **6** over an ISI. Integrals, such as

$$\int_t^{t+\Delta t_{ISI}} k_2 \cdot SP_{LS}(t) \cdot dt = \int_t^{t+\Delta t_{ISI}} (k_{2,rest} + \sigma_2 \cdot ([Ca^{2+}](t) - [Ca^{2+}]_{rest})) \cdot SP_{LS}(t) \cdot dt \quad (10)$$

can be approximated by

$$(\Delta t_{ISI} \cdot k_{2,rest} + s_2) \cdot \overline{SP}_{LS} \quad (11)$$

where Δt_{ISI} is the duration of the ISI, $\overline{SP}_{LS}$ is the mean value of $SP_{LS}(t)$ over the entire ISI, and

$$s_2 = \int_t^{t+\Delta t_{ISI}} \sigma_2 \cdot ([Ca^{2+}](t) - [Ca^{2+}]_{rest}) \cdot dt \quad (12)$$

For frequencies ≤20 Hz, AP-induced $[Ca^{2+}]$ transients decay back to $[Ca^{2+}]_{rest}$ during the ISI. In that case, s_2 represents the fraction of an upstream SV subpool transferred by the AP to the respective downstream pool (in this case from SP_{LS} to SP_{TS}). At frequencies ≥50 Hz, when $[Ca^{2+}]$ transients extend over several ISIs, this fraction is distributed over these ISIs.

An equation analogous to Eq. **12** also holds for s_1, the fraction of empty sites being filled during an AP. Approximating $SP_{LS}(t)$ in Eq. **10** by $\overline{SP}_{LS}$ requires that changes in SP_{LS} during one ISI are relatively small. This requirement is satisfied quite well at the steady-state of eEPSC trains and for values of s_1 and s_2 of ~0.1. Constants, such as b_1 and b_2, as well as the constant parts of k_1 and k_2, i.e. $k_{1,rest}$ and $k_{2,rest}$, show up in the low-frequency approximation as products of Δt_{ISI} and their respective values (Eq. **11**). Performing these integrations over an ISI, we arrive at the following difference equations for the changes in SV subpool sizes (ΔSP_{LS} and ΔSP_{TS}) during one ISI:

$$\begin{aligned}\Delta SP_{LS} = & -\left[\Delta t_{ISI} \cdot \left(b_1 + k_{1,rest} + k_{2,rest}\right) + s_1 + s_2\right] \cdot \overline{SP}_{LS} \\ & + \left[\Delta t_{ISI} \cdot \left(b_2 - k_{1,rest}\right) - s_1\right] \cdot \overline{SP}_{TS} + \left[\Delta t_{ISI} \cdot k_{1,rest} + s_1\right] \cdot N_{tot}\end{aligned} \quad (13)$$

$$\Delta SP_{TS} = \left(\Delta t_{ISI} \cdot k_{2,rest} + s_2\right) \cdot \overline{SP}_{LS} - \left(\Delta t_{ISI} \cdot b_2 + p_{fusion}\right) \cdot \overline{SP}_{TS} \quad (14)$$

In Eq. **14** we include as a decrement the number of SV_{TS}s fusing in response to an AP ($m = p_{fusion} \cdot \overline{SP}_{TS}$), such that ΔSP_{TS} represents the total change in SP_{TS} during one ISI. Here we introduce another simplification because the number of SV_{TS}s fusing (m) is actually proportional to the product of p_{fusion} with the size of SP_{TS} at the time of arrival of stimulus j ($SP_{TS,j}$), i.e. immediately before the beginning of the subsequent ISI. However, again the relative magnitude of this error $(SP_{TS,j} - \overline{SP}_{TS})/\overline{SP}_{TS}$ is small at steady-state.

Solving for the mean steady-state size of SV subpools SP_{LS} ($\overline{SP}_{LS,ss}$) and SP_{TS} ($\overline{SP}_{TS,ss}$) by setting ΔSP_{LS} and ΔSP_{TS} in Eqs. **13** and **14** to 0, we obtain:

$$\overline{SP}_{LS,ss} = N_{tot} \cdot (\Delta t_{ISI} \cdot k_{1,rest} + s_1) \cdot (\Delta t_{ISI} \cdot b_2 + p_{fusion})/S \quad (15)$$

and

$$\overline{SP}_{TS,ss} = N_{tot} \cdot (\Delta t_{ISI} \cdot k_{2,rest} + s_2) \cdot (\Delta t_{ISI} \cdot k_{1,rest} + s_1)/S \quad (16)$$

where

$$S = \left(\Delta t_{ISI} \cdot b_2 + p_{fusion}\right) \cdot \left(\Delta t_{ISI} \cdot \left(b_1 + k_{1,rest} + k_{2,rest}\right) + s_1 + s_2\right) \quad (17)$$

$$-(\Delta t_{ISI} \cdot k_{2,rest} + s_2) \cdot (\Delta t_{ISI} \cdot (b_2 - k_{1,rest}) - s_1)$$

Eq. **16** can be used to calculate the relative steady-state depression of release during eEPSC trains, defined as

$$D_m = m_{ss}/m_1 \approx p_{fusion,ss}/p_{fusion,1} \cdot \overline{SP}_{TS,ss}/SP_{TS,1}. \quad (18)$$

It represents a good estimate for D_m *in* the frequency range 1 to 20 Hz, once the parameters involved are known. In the next paragraph we describe how most of these can be determined form the experimental data.

Prediction of readily measurable quantities at stimulus frequencies of 5 to 20 Hz

For f_{stim} = 5–20 Hz, D_m approaches an asymptotic value because the terms $\Delta t_{ISI} \cdot k_{1,rest}$ and $\Delta t_{ISI} \cdot k_{2,rest}$ are smaller by an order of magnitude than s_1 and s_2. In addition, $\Delta t_{ISI} \cdot b_1$ and $\Delta t_{ISI} \cdot b_2$ are much smaller than the products of Δt_{ISI} and $k_{1,rest}$ and $k_{2,rest}$. Thus, SVs priming proceeds predominantly from left to right in the schemes of Fig. 1. Neglecting the small terms, one arrives at two very simple equations for the increments in SV subpool sizes in analogy to Eqs. **13** and **14**

$$\Delta SP_{LS} = -(s_1 + s_2) \cdot \overline{SP}_{LS} - s_1 \cdot \overline{SP}_{TS} + s_1 \cdot N_{tot} \quad (19)$$

$$\Delta SP_{TS} = s_2 \cdot \overline{SP}_{LS} - p_{fusion} \cdot \overline{SP}_{TS} \quad (20)$$

These equations, together with

$$\overline{N}_{e,ss} + \overline{SP}_{LS,ss} + \overline{SP}_{LS,ss} = N_{tot} \quad (21)$$

define the steady-state values of the SV subpool sizes ($\overline{SP}_{LS,ss}$ and $\overline{SP}_{TS,ss}$) according to:

$$\overline{SP}_{LS,ss} = N_{tot}/s_2/\left(\frac{1}{p_{fusion,ss}} + \frac{1}{s_1} + \frac{1}{s_2}\right) \quad (22)$$

$$\overline{SP}_{TS,ss} = N_{tot}/p_{fusion,ss}/\left(\frac{1}{p_{fusion,ss}} + \frac{1}{s_1} + \frac{1}{s_2}\right) \quad (23)$$

The quantal content of the steady-state eEPSC (m_{ss}) can be approximated by

$$m_{ss} \approx \overline{SP}_{TS,ss} \cdot p_{fusion,ss} = N_{tot} / \left(\frac{1}{p_{fusion,ss}} + \frac{1}{s_1} + \frac{1}{s_2} \right) \quad (24)$$

Equations 22–24 and other readily available data were used to derive initial guesses for model parameters.

A simpler form for calculating the mean steady-state size of SP_{LS} is obtained by setting ΔSP_{TS} in Eq. **20** to 0:

$$\overline{SP}_{LS,ss} = p_{fusion} \cdot \overline{SP}_{TS,ss} / s_2 \quad (25)$$

By considering that $p_{fusion} \cdot \overline{SP}_{TS,ss} = m_{ss}$ and $m_{ss} = m_1 \cdot D_m$, and introducing D_{LS}, the relative occupancy of SP_{LS} at steady state ($D_{LS} = \overline{SP}_{LS,ss} / SP_{LS,1}$), we obtain:

$$SP_{LS,1} = \frac{m_1}{s_2} \cdot \frac{D_m}{D_{LS}} \quad (26)$$

Similarly, a simple expression for the paired-pulse ratio (*PPR*), calculated from the two initial eEPSCs in a train, can be obtained as:

$$PPR = \frac{m_2}{m_1} = \frac{p_{fusion,2} \cdot SP_{TS,2}}{m_1} \quad (27)$$

Applying Eq. **20** to eliminate $SP_{TS,2}$, we obtain:

$$PPR = p_{fusion,1} \cdot r_p \cdot (SP_{TS,1} \cdot (1 - p_{fusion,1}) + s_2 \cdot SP_{LS,1}) \cdot \frac{1}{m_1} \quad (28)$$

Here, the parameter $r_p = p_{fusion,2} / p_{fusion,1}$ was introduced, which is very close to 1 for low-frequency stimulation. Considering that $p_{fusion,1} \cdot SP_{TS,1} = m_1$, and using Eq. **26** to eliminate $SP_{LS,1}$ we obtain

$$PPR = r_p \cdot (1 - p_{fusion,1} \cdot (1 - \frac{D_m}{D_{LS}})) \quad (29)$$

This equation can be used to calculate $p_{fusion,1}$:

$$p_{fusion,1} = (1 - \frac{PPR}{r_p}) / (1 - \frac{D_m}{D_{LS}}) \quad (30)$$

Because r_p is very close to 1 for 10 Hz stimulation, and because only little reduction in the size of SP_{LS} is observed during trains at 10 Hz (Fig. 4B1), an approximate expression for p_{fusion}, assuming $r_p \approx 1$ and $D_{LS} \approx 1$, is simply:

$$p_{fusion,1} \approx (1 - PPR)/(1 - D_m) \tag{31}$$

In conclusion, provided that $p_{fusion,2}$ is close to $p_{fusion,1}$ and that $SP_{LS,ss}$ is close to $SP_{LS,1}$, Eq. **31** can be used to calculate $p_{fusion,1}$ from two readily determined experimental quantities: the *PPR* and the relative steady-state depression D_m. It should be noted, that the stated conditions are fulfilled at the calyx synapse for 10 Hz, but not necessarily at other types of synapses and at the same frequency.

Estimates for parameters s_1 and s_2 .

As shown previously (8; their Fig. 8), Eqs. **13** and **14** can be used to simulate the time course of BF_{LS} as a function of the two model parameters p_{fusion} and s_2, the latter being designated as α in that publication. Assuming that p_{fusion} is constant and known from two-component NTF, we used this possibility to obtain an estimate for s_2 by fitting simulated BF_{LS}, to the BF_{LS}, as obtained from a three-component NTF. An alternative estimate can be obtained by solving Eq. **26** for s_2, assuming a value close to 1 for D_{LS}, as suggested by NTF. The two methods provide very similar values close to 0.1.

Given this estimate for s_2, Eq. **24** can be solved for s_1:

$$s_1 = m_{ss} \Big/ \left(N_{tot} - m_{ss} \cdot \left(\frac{1}{p_{fusion,ss}} + \frac{1}{s_2} \right) \right) \tag{32}$$

Except for N_{tot}, all quantities on the right-hand side of this equation are known. We noticed that model fits do not vary in a major way, when using s_1 calculated with Eq. **32** and setting N_{tot} to values which result in 20% to 30% empty release sites at rest. Thus, we calculated the initial guess for s_1 according to Eq. **32** with N_{tot} set to $1.25 \cdot (M_{LS} + M_{TS})$.

Initial guess values for model parameters describing the resting state

In order to define a complete set of initial guess values for model fitting, four more parameters, $k_{1,rest}$, $k_{2,rest}$, b_1 and b_2, describing the resting state, must be determined. Eqs. **7**–**9** provide two constraints on the choice of these parameters. The choice of $k_{1,rest}$ strongly influences the time course of recovery from depression induced by conditioning stimulation. It was therefore used as a free parameter during model fitting, and adjusted to yield a time constant of recovery from STD following low-frequency stimulation of 4–6 s (13). In addition, we found that at low frequencies, the slope of the relationship between steady-state depression and f_{stim} was fitted appropriately if the characteristic frequency for the second priming step (ratio $k_{2,rest} / s_2$) was chosen somewhat lower than that of the first one (ratio $k_{1,rest} / s_1$). With

$$k_{2,rest}/s_2 = 0.5 \cdot k_{1,rest}/s_1, \quad (33)$$

$SP_{LS,rest} = M_{LS}$, $SP_{TS,rest} = M_{TS}$ and Eq. **1**, we get from Eq. **8**:

$$b_1 = N_{e,rest} \cdot k_{1,rest}/SP_{LS,rest}. \quad (34)$$

From Eq. **33**:

$$k_{2,rest} = k_{1,rest} \cdot s_2/s_1 \quad (35)$$

From Eq. **9**:

$$b_2 = SP_{LS,rest} \cdot k_{2,rest}/SP_{TS,rest} \quad (36)$$

It is important to note that Eqs. **8**–**36** are approximations, based on strict linearity of the system, such as constancy of certain parameters and linear dependence of priming rate constants on [Ca^{2+}] (but see Discussion on this requirement). Nevertheless, we found that assigning initial guess values derived this way to the model parameters resulted in good fits to experimental data obtained with 1–20 Hz stimulation even without further parameter optimization (see Results section). Yet, most of them were used as free parameters in subsequent trial and error fitting.

Local [Ca^{2+}] transients and release probability

Release per action potential is a power function of the local [Ca^{2+}] 'seen' by the Ca^{2+} sensor for release (14, 15). We therefore determined $p_{fusion,j}$, the release probability at arrival of the j^{th} AP, according to

$$p_{fusion,j} = p_{fusion,1} \cdot {y_j}^{4.5} \cdot z_j \quad (37)$$

with y≥1 and z≤1. Here, $p_{fusion,1}$ designates the fusion probability for the first eEPSC in a train (Table 1), y_j accounts for changes in local [Ca^{2+}] during repetitive stimulation ($y_j = [Ca^{2+}]_j/[Ca^{2+}]_1$), likely due to presynaptic Ca^{2+} current facilitation (16, 17), and/or saturation of local Ca^{2+} buffers (18-20). z accounts for a reduction of p_{fusion} during repetitive stimulation, as indicated by NTF analysis, which, however, was relatively small. A candidate mechanism generating a small decrease in mean p_{fusion} during trains could be a slightly non-uniform p_{fusion} among all SV_{TS}s of a given synapse.

Both variables y_j and z_j were initialized to 1 at the onset of a stimulus train. The variable y was incremented after each AP by

$$y_{inc} = y_{inc,1} \cdot (y_{max} - y_j) \quad (38)$$

and *z* was decremented by

$$z_{dec} = z_{dec,1} \cdot (z_j - z_{min}) \quad (39)$$

During ISIs, both *y(t)* and *z(t)* were solved numerically, together with other model parameters (see Eqs. **2**, **3**), according to

$$\frac{d}{dt}\, y(t) = (1 - y(t)) \cdot k_y \quad (40)$$

$$\frac{d}{dt}\, z(t) = (1 - z(t)) \cdot k_z \quad (41)$$

The parameters describing *y(t)*, $y_{inc,1}$, y_{max} and k_y, were initialized with previously published values (21) and adjusted by trial and error fitting. The parameters describing *z(t)*, $z_{dec,1}$, z_{min} and k_z, were initialized to values, which would produce a decrease of p_{fusion} of ≤15% during the first few APs at 10 Hz. All six parameters of the *y-z* formalism were then adjusted during trial-and-error fitting to reproduce the time course of p_{fusion} as derived from NTF analysis (Fig. 3D). The p_{fusion} time courses show a small negative trend for the 5–20 Hz average trace due to a decrease in the *z* variable and quite prominent facilitation for 200 Hz due to an increase in the *y* variable. Reliable NTF-derived p_{fusion} estimates can only be obtained for the initial four eEPSCs from BF_{TS}. Later during trains, BF_{TS} is very small, such that estimates are unfortunately dominated by random fluctuations. Once all six parameters of the *y-z* formalism were determined on the basis of the BF_{TS}, they were held constant during all numerical simulations of release and STP.

Extensions of the 'Simple' sequential kinetic scheme to reproduce high frequency features

In order to simulate the experimentally observed time courses at f_{stim} ≥50 Hz, the linear model as presented above (Fig.1B) had to be extended. This can be achieved in several ways, as explained in the Results section. In our preferred variant, described here in detail, we introduced an additional fusion-competent SV state, which is similar to state TS but labile (TSL, Fig. 1C). SVs populating this state (SV_{TSL}s) after an AP rapidly relax to state LS due to a relatively high backward rate constant b_3. The experimentally observed saturation of release at high f_{stim} (suppl. Fig. 1C) can be described in two alternative ways. Here, for completeness, we describe how both extensions were handled, although most of the results presented were obtained by simply introducing Michaelis-Menten (MM) like saturation of k_1 according to:

$$k_1(t) = \left(k_{1,rest} + \sigma_1 \cdot ([Ca^{2+}](t) - [Ca^{2+}]_{rest})\right) / \left(1 + ([Ca^{2+}](t) - [Ca^{2+}]_{rest}) / K_{0.5)}\right) \quad (42)$$

Alternatively, an additional empty and refractory state (ERS) can be introduced as shown in Fig. 1C2). The extended scheme, including the ERS, is described in analogy to Eqs. **1**–**6** by:

$$\frac{d}{dt} SP_{LS}(t) = -(b_1 + k_1 + k_2) \cdot SP_{LS}(t) + (b_2 - k_1) \cdot SP_{TS}(t) + (b_3 - k_1) \cdot SP_{TSL}(t) - k_1 \cdot N_{ERS}(t) + N_{tot} \cdot k_1 \quad (43)$$

$$\frac{d}{dt} SP_{TS}(t) = k_2 \cdot SP_{LS}(t) - b_2 \cdot SP_{TS}(t) \quad (44)$$

$$\frac{d}{dt} SP_{TSL}(t) = -b_3 \cdot SP_{TSL}(t) \quad (45)$$

$$\frac{d}{dt} N_{ERS}(t) = -b_4 \cdot N_{ERS}(t) \quad (46)$$

As in the case of the basic model, differential equations Eqs. **43**–**46** together with Eqs. **6**, **40**, and **41** were solved numerically between APs and decrements/increments were applied subsequent to each AP. Release was calculated as $(SP_{TS}(t) + SP_{TSL}(t)) \cdot p_{fusion}$.

The two parameters describing $SP_{TSL}(t)$ were κ, the fraction of SP_{LS} transferred to SP_{TSL} per AP and a backward rate constant b_3. Both parameters were determined by trial-and-error fitting, aiming at a correct representation of amount and time course of quantal release. For convenience, the same program code can be used for both model options of handling release saturation. For the case of Michaelis-Menten-type saturation b_4 can be set to a very high value (≥5000 s^{-1}) to prevent filling of ERS while adjusting $K_{0.5}$. Alternatively, $K_{0.5}$ can be set to 10 M while adjusting b_4.

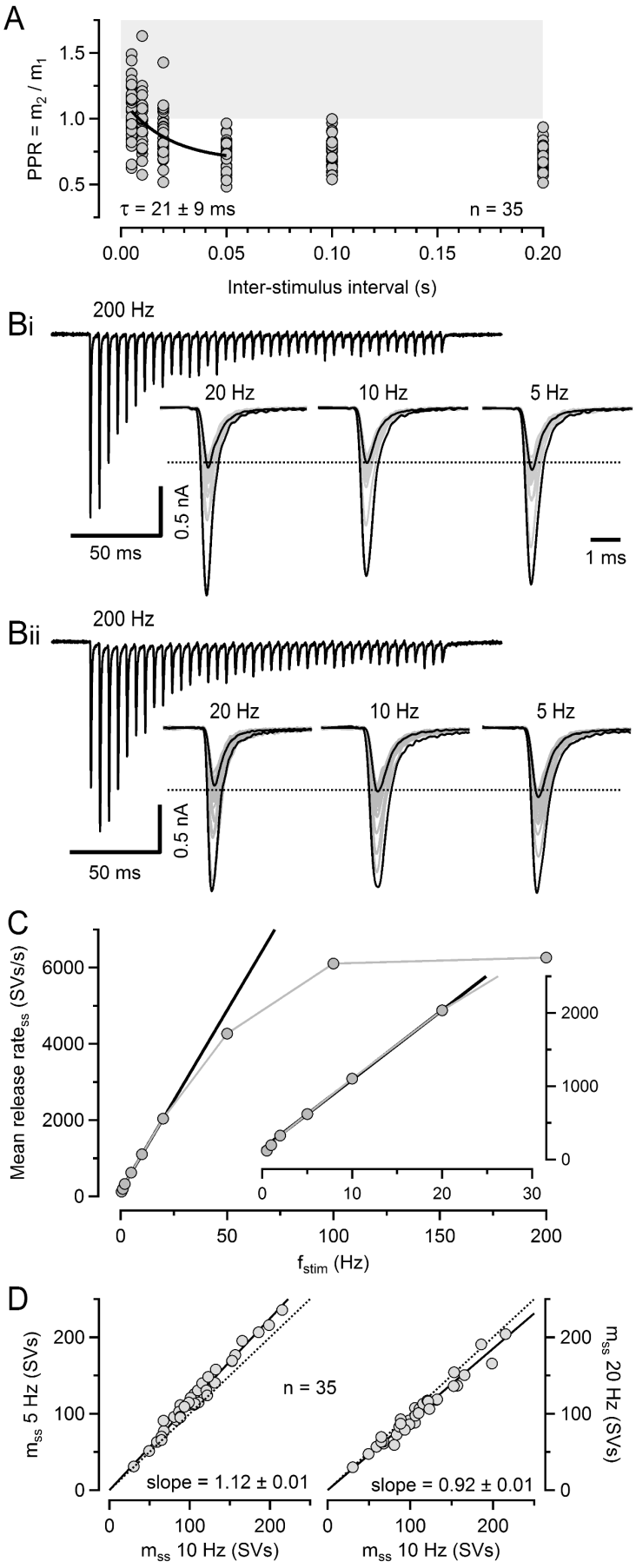
A
PPR = m2 / m1
1.5
1.0
0.5
τ = 21 ± 9 ms
n = 35
0.00
0.05
0.10
0.15
0.20
Inter-stimulus interval (s)
Bi
200 Hz
20 Hz
10 Hz
5 Hz
0.5 nA
50 ms
1 ms
Bii
200 Hz
20 Hz
10 Hz
5 Hz
0.5 nA
50 ms
C
Mean release rate_ss (SVs/s)
6000
4000
2000
0
2000
1000
0
0
10
20
30
0
50
100
150
200
f_stim (Hz)
D
m_ss 5 Hz (SVs)
200
100
0
n = 35
slope = 1.12 ± 0.01
slope = 0.92 ± 0.01
0
100
200
m_ss 10 Hz (SVs)
m_ss 20 Hz (SVs)

Fig. S1. Characterization of *PPR*s and steady-state release.
***A*.** *PPR*s = m_2 / m_1 plotted vs. ISI for all 35 synapses. The solid line represents an exponential fit to the data in the ISI range from 5–50 ms yielding a time constant of 21 ± 9 ms.
B*.** Example eEPSC trains recorded in a depressing (B*, *i***) and a facilitating (***B*, *ii***) synapse stimulated at 200 Hz (top panels) and 20, 10 and 5 Hz (bottom panels). For 5–20 Hz trains, eEPSCs are shown superimposed and $eEPSC_2$ to $eEPSC_{29}$ are shown in gray. Note the similar $eEPSC_{ss}$ amplitudes for 5–20 Hz stimulation (dotted lines).
***C*.** Mean steady-state release rate ($m_{ss} \cdot f_{stim}$) plotted versus f_{stim}. The solid black line represents a linear regression to the f_{stim} range 2–20 Hz, which is shown at an expanded abscissa in the inset.
***D*.** Scatter graphs of m_{ss} for 5 Hz (left) and for 20 Hz (right) versus the corresponding m_{ss} for 10 Hz stimulation for all 35 synapses. Note the close proximity of linear regressions to the identity lines. On average, m_{ss} was only 12% larger or only 8% smaller for 5 and 20 Hz, respectively, when compared to the corresponding 10 Hz m_{ss} values.

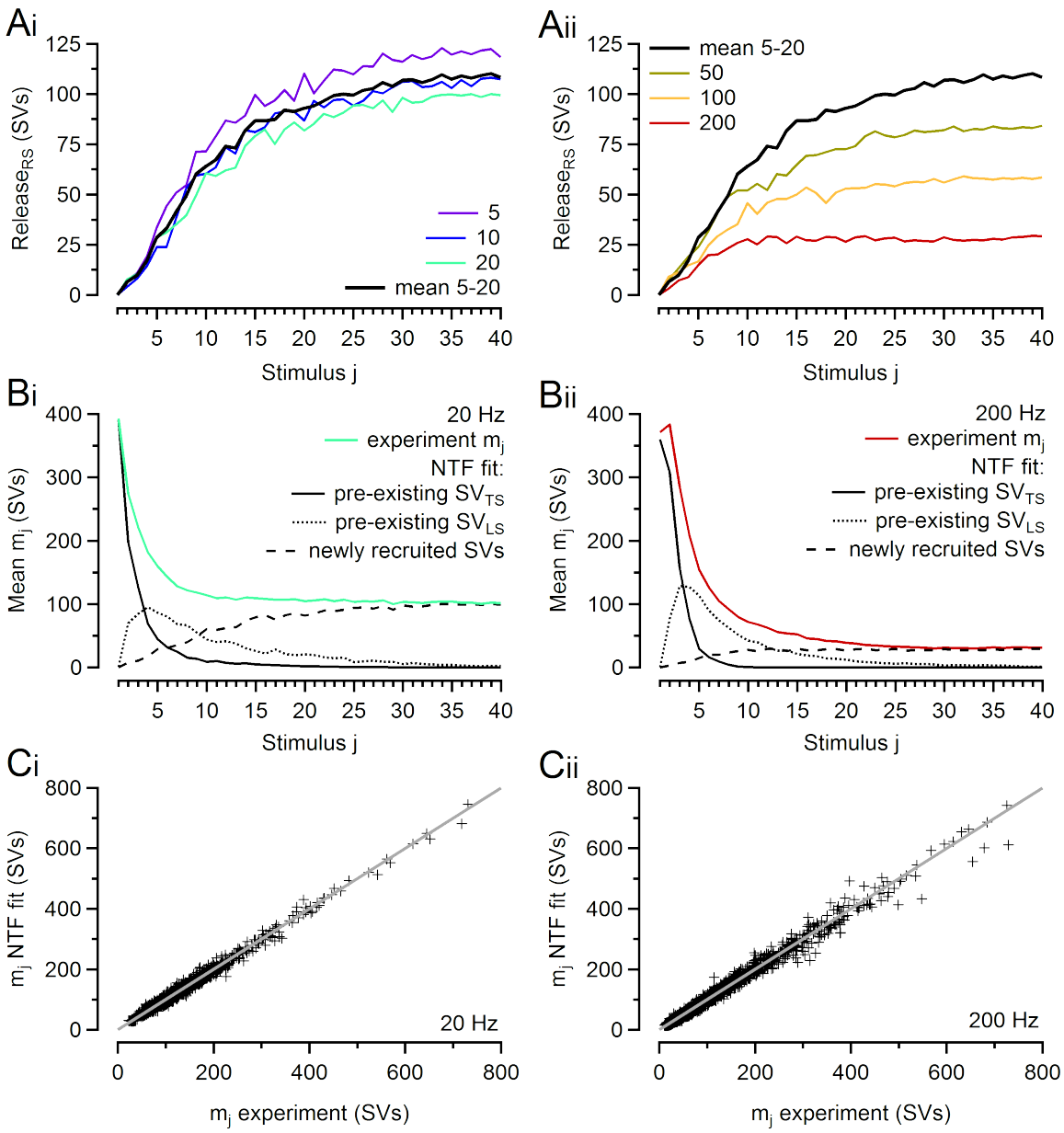

Fig. S2. Three-component NTF decomposition analysis.
A. Contributions to release by newly recruited SVs (mean $M_{RS} \cdot BF_{RS,j}$) for low (***A, i***) and high (***A, ii***) f_{stim}. The black traces in ***A, i*** and ***A, ii*** represent the mean time course for 5–20 Hz. The time courses represent release contributed by SVs, which dock to empty sites during trains and undergo the sequence of two-step priming and fusion. They start in a sigmoid fashion and approach a steady-state.
B. Mean m_j values (solid colored traces) versus stimulus index j for 20 Hz (***B, i***) and 200 Hz (***B, ii***). NTF fit derived mean release components contributed by either preexisting SV$_{TS}$s (mean $M_{TS} \cdot BF_{TS,j}$, solid black line), preexisting SV$_{LS}$s (mean $M_{LS} \cdot BF_{LS,j}$, dotted black line) and newly recruited SVs (mean $M_{RS} \cdot BF_{RS,j}$, dashed black line) are shown superimposed. Note that all preexisting SV$_{TS}$s and all preexisting SV$_{LS}$s are nearly completely consumed within the initial 8 and 30 APs, respectively. For stimuli ≥30, release is nearly exclusively supported by newly-recruited SVs.
C. Scatter plot of individual m_j for all stimuli *j* in all synapses as estimated by NTF decomposition analysis versus the respective experimentally measured values for 20 Hz (***C, i***) and 200 Hz (***C, ii***). Note that the values are very close to the identity line and approximately symmetrically distributed around it (light gray).

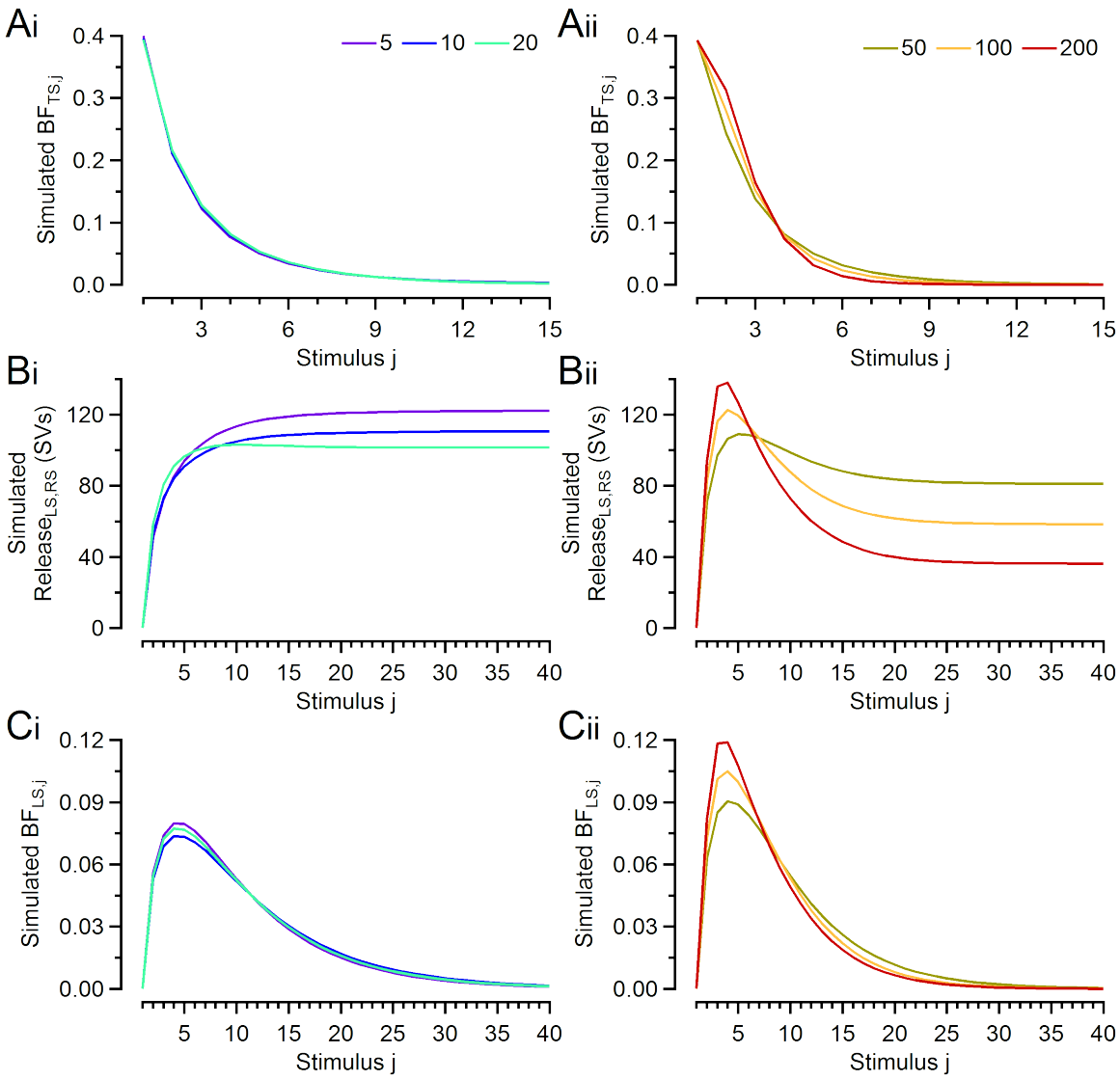

Fig. S3. Model-derived predictions for NTF basefunctions.
A. Simulated BF_{TS} time courses for f_{stim} 5, 10 and 20 Hz (***A, i***) and 50, 100 and 200 Hz (***A, ii***) (compare to Fig. 3A).
B. Simulated mean $M_{LS,RS} \cdot BF_{LS,RS}$ release time courses for f_{stim} 5, 10 and 20 Hz (***B, i***) and 50, 100 and 200 Hz (***B, ii***) (compare to Fig. 3B).
C. Simulated BF_{LS} time courses for f_{stim} 5, 10 and 20 Hz (***C, i***) and 50, 100 and 200 Hz (***C, ii***) (compare to Fig. 3C).
For all simulation shown in ***A***–***C***, default model parameters (Table 1) were used.

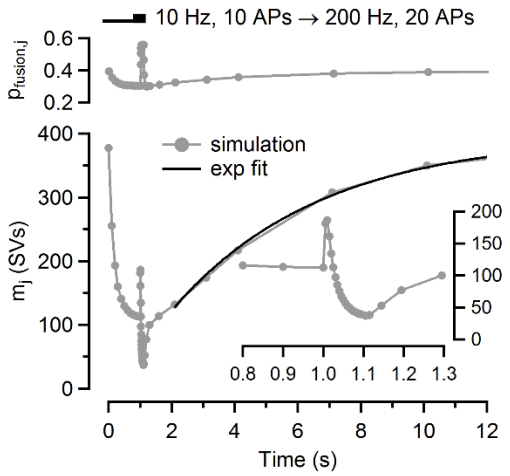

Fig. S4. Simulation of a complex stimulus pattern including a switch of f_{stim} from 10 to 200 Hz and several single stimuli delivered at various intervals to probe the time course of recovery from STD
Simulated mean m_j values for a stimulus pattern consisting of 10 conditioning stimuli at 10 Hz followed by a regular 200 Hz train consisting of 20 stimuli. Thereafter, recovery of m_j was probed with single stimulus delivered at increasing recovery intervals (0.01, 0.02, 0.05, 0.1, 0.2, 0.5, 1, 2, 3, 6, 9 s). The black line represents a single exponential fit yielding a time constant of ~4.7 s. The inset shows the time course of m_j around the onset of 200 Hz stimulation at higher time resolution. The simulated time course of p_{fusion} is plotted in the small panel on top.
The model predicts substantial depression during the 10 Hz episode (m_{10} / m_1 = 0.301). Upon onset of 200 Hz stimulation, strong facilitation is observed (*PPR* m_{12} / m_{11} = 1.61), which quickly turns into more severe depression (m_{30} / m_1 = 0.104). A *PPR* of 1.61 is considerably larger than the respective average *PPR* observed without preconditioning (m_2 / m_1 = 1.07 ± 0.03). The predicted p_{fusion} (Fig. 5E upper panel) decreases during 10 Hz stimulation by 23%, which is followed during 200 Hz stimulation by a transient increase above $p_{fusion,1}$ (42%). Decrease and increase in p_{fusion} are generated by the time courses of z (Eqs. **39**, **40**) and y (Eqs. **38**, **40**), respectively. At the end of the 200 Hz episode, both parameters revert to their resting values as determined by the rate constants k_y and k_z (Eqs. **40**, **41**; Table S2). It should be noted, that the predicted changes in p_{fusion} are largely based on an empirical model, which reproduces NTF results (Fig 3D).

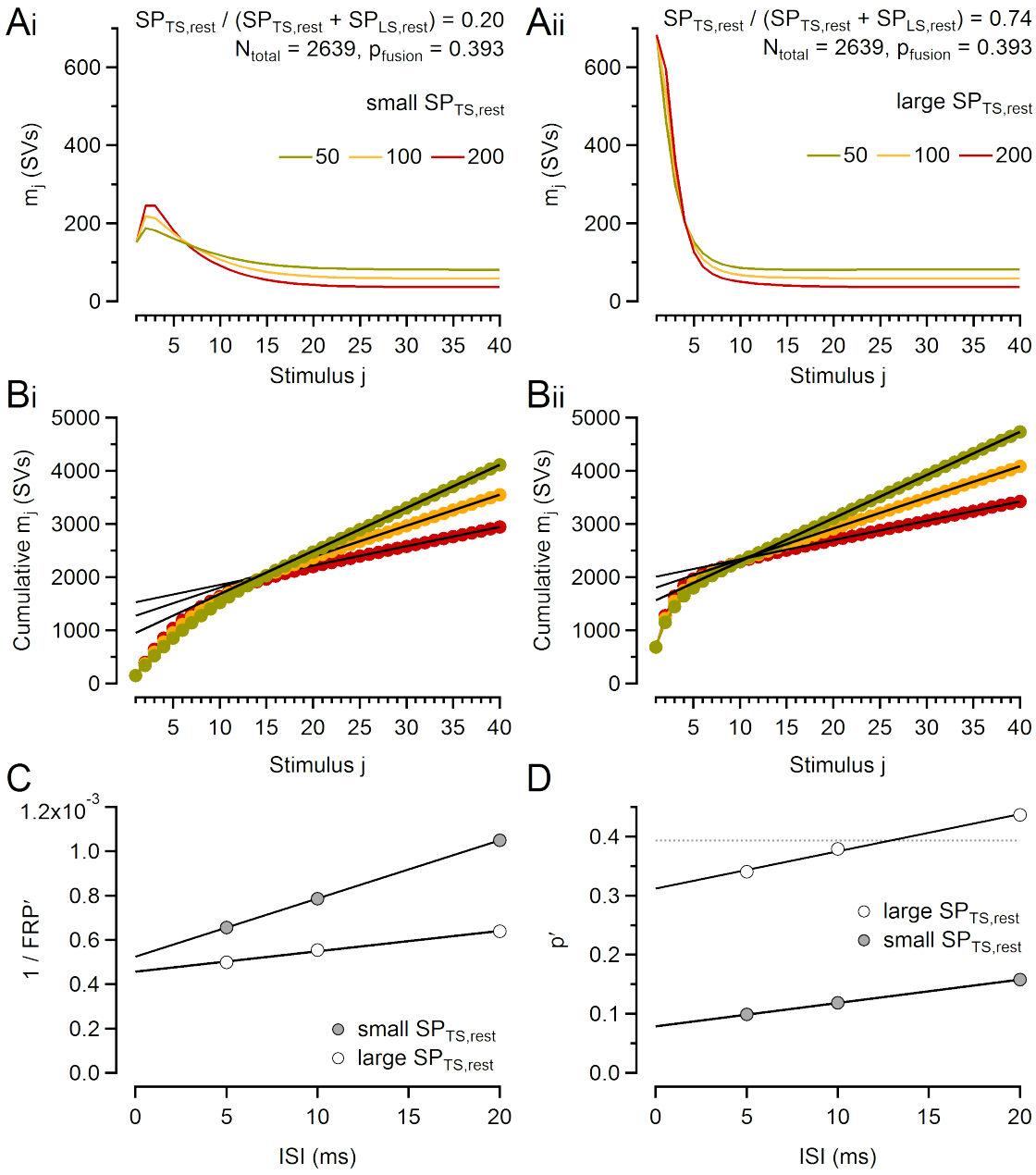

Fig. S5. 'Traditional' *FRP* and *p* analysis of simulated eEPSC trains for synapses with different $SP_{TS,0}$ fractions misinterprets differences in STP.

A. Time courses of m_j in response to 50, 100 and 200 Hz stimulation simulated using standard values for all model parameters except for b_2 which was either increased (***A, i***) or decreased (***A, ii***) such that the fraction $SP_{TS,0}$ / ($SP_{LS,0}$ + $SP_{TS,0}$) was reduced to ~20% or enhanced to ~74%, respectively (replotted from Fig. 6C).

B. *FRP'* estimates obtained from cumulative m_j for f_{stim} = 50, 100 and 200 Hz for the two simulations shown in ***A***.

C. Corrected *FRP* estimates derived from back-extrapolations to infinite f_{stim} (ISI = 0 ms) were similar and amounted to 1908 SVs and 2193 SVs for the simulations shown in ***A, i*** and ***A, ii***, respectively. These corrected *FRP* estimates compare favorably to the respective sum $SP_{LS,0}$ + $SP_{TS,0}$ which amounted to 1929 SVs (simulation ***A, i***) and to 2356 SVs (simulation ***A, ii***).

D. Corrected 'traditional' *p* estimates derived from the ratios m_1 / *FRP'* differ nearly fourfold for the simulations shown in ***A, i*** ('traditional' p = 0.079) and ***A, ii*** ('traditional' p = 0.312), despite using the same p_{fusion} value

during simulations. For the sequential two-step priming scheme (Fig. 1B), a 'traditional' p estimate equals $p_{fusion} \cdot SP_{TS,0} / (SP_{LS,0} + SP_{TS,0})$, corresponding to $0.39 \cdot 0.20 = 0.078$ (simulation ***A, i***) and to $0.39 \cdot 0.74 = 0.290$ (simulation ***A, ii***).

Table S1. List of abbreviations and symbols

Abbreviations and symbols as shown here may appear in the text with the letter 's' appended, which indicates plural. A subscript 'rest' denotes a value of the respective quantity at resting state, i.e. in the absence of presynaptic action potentials. On occasion, subscripts may have suffixes which denote indices of arrays.

Abbreviation or symbol	Definition
kyn	Kynurenic acid, competitive antagonist with a fast off rate, counteracting AMPAR desensitization and saturation
AP	action potential
VGCC	voltage-gated Ca^{2+} channel
$eEPSC_j$	AP-evoked excitatory postsynaptic current in response to the j^{th} stimulus
m_j	quantal content (number of SVs) released during $EPSC_j$
m_{ss}	quantal content at steady state, i.e. at the end of a stimulus train
D_m	steady state depression, i.e. m_{ss} / m_1
PPR	paired-pulse ratio, i.e. $eEPSC_2 / eEPSC_1 = m_2 / m_1$
ISI	inter-stimulus interval, i.e. interval between two consecutive stimuli
$[Ca^{2+}]$	concentration of intracellular Ca^{2+} ions
SV	synaptic vesicle
FRP	fast releasing pool of SVs, a SV subpool in calyx terminals which accounts for the majority of the AP-evoked release (22, 23)
SRP	slowly releasing pool of SVs, a SV subpool in calyx terminals which contributes little to AP-evoked release but is recruited for example during long depolarizations (22, 23)
TS	'tightly docked state' of a SV which is fusion-competent
TSL	a SV state similar to TS but labile
LS	'loosely docked state' of a SV which is not fusion-competent
ES	empty state of a release site
ERS	empty and refractory state of a release site
SV_{TS}	synaptic vesicle currently in TS
SV_{TSL}	synaptic vesicle currently in TSL
BF	basefunction returned by an NTF decomposition fit, representing the normalized time course of quantal release during a stimulus train contributed by a specific fraction of SVs, which were in a certain state immediately prior to stimulation
BF_{TS}	basefunction representing normalized time course of release contributed by those SVs that were in TS immediately prior to stimulation
BF_{LS}	basefunction representing normalized time course of release contributed by those SVs that were in LS immediately prior to stimulation
BF_{LS}	basefunction representing normalized time course of release contributed by those SVs that were in LS immediately prior to stimulation
BF_{RS}	basefunction representing normalized time course of release contributed by those SVs that were neither in TS nor in LS immediately prior to stimulation but are newly recruited and released during a stimulus train
$BF_{LS,RS}$	basefunction representing the sum of BF_{LS} plus BF_{RS}, as returned by a two-component NTF decomposition fit
p_{fusion}	SV fusion probability, i.e. the probability of a docked and fusion-competent SV of undergoing fusion during a single AP
SP_{TS}	subpool of SV_{TS}s, i.e. all SVs in TS at any given moment
SP_{TSL}	subpool of SV_{TSL}s, i.e. all SVs in TSL at any given moment
SP_{LS}	subpool of SV_{LS}s, i.e. all SVs in LS at any given moment
N_e	number of empty release sites
N_{total}	total number of release sites
N_{ERS}	number of empty and refractory release sites
M	quantal content of an entire eEPSC train, i.e. the sum of all SVs contributing to release during the entire stimulus train
M_{TS}	fraction of M representing those SVs that had been in TS prior to stimulation; M_{TS} represents the entire subpool of SV_{TS}s (SP_{TS}) available for release immediately prior to stimulation if a stimulus train is long enough such that BF_{TS} decays to 0
M_{LS}	fraction of M representing those SVs that had been in LS immediately prior to stimulation analog to M_{TS}
M_{RS}	fraction of *M* representing those SVs that had been neither in TS nor in LS immediately prior to stimulation but are newly recruited and released during a stimulus train
$M_{LS,RS}$	fraction of *M* representing those SVs that had been either in LS immediately prior to stimulation or else are newly recruited and released during a stimulus train

Table S2. Model parameter descriptions and parameter values for the sequential two-step priming and fusion scheme.

Model parameter description	Symbol	Initial guess[1]	MM model variant[2]	ERS model variant[3]
Size of tightly-docked SV subpool at rest	$SP_{TS,rest}$	NTF	961	961
Size of loosely-docked SV subpool at rest[4]	$SP_{LS,rest}$	NTF	1150	1150
Total number of release sites	N_{tot}	NTF	2639	2639
Initial fusion probability	$p_{fusion,1}$	NTF	0.39	0.39
Rate constant for the ES → LS transition at rest	$k_{1,rest}$		0.4025 s^{-1}	0.4025 s^{-1}
Ca^{2+} dependence of the ES → LS transition	σ_1		$s_1 \cdot k_{Ca}/\Delta[Ca^{2+}]$	$s_1 \cdot k_{Ca}/\Delta[Ca^{2+}]$
Fraction of empty sites transferred to SP_{LS} by an AP[5]	s_1	NTF	0.0818	0.0818
Rate constant for the ES ← LS transition	b_1		0.1847 s^{-1}	0.1847 s^{-1}
Rate constant for the LS → TS transition at rest	$k_{2,rest}$		0.2073 s^{-1}	0.2073 s^{-1}
Ca^{2+} dependence of the LS → TS transition	σ_2		$s_2 \cdot k_{Ca}/\Delta[Ca^{2+}]$	$s_2 \cdot k_{Ca}/\Delta[Ca^{2+}]$
Fraction of SP_{LS} transferred to SP_{TS} by an AP[5]	s_2	NTF	0.0843	0.0843
Rate constant for the LS ← TS transition	b_2		0.248 s^{-1}	0.248 s^{-1}
Fraction of SP_{LS} transferred to SP_{TSL} by an AP	κ		0.16	0.16
Decay time constant of the TSL state, inverse of the rate constant for the LS ← TSL transition	$1 / b_3$		90 ms	90 ms
Rate constant for the ERS → ES transition	b_4		5000 s^{-1}	3.6 s^{-1}
Basal $[Ca^{2+}]$ at rest	$[Ca^{2+}]_{rest}$		50 nM	50 nM
$[Ca^{2+}]$ increment per AP-induced 'effective' $[Ca^{2+}]$ transient	$\Delta[Ca^{2+}]$		110 nM	110 nM
Decay time constant of the AP-induced 'effective' $[Ca^{2+}]$ transient	$1 / k_{Ca}$		60 ms	60 ms
Michaelis-Menten K_D of the ES → LS transition	$K_{0.5}$		280 nM	10 M
Exponent of power law of facilitation variable y			4.5	4.5
Decay time constant of the facilitation variable y	$1 / k_y$	NTF	14 ms	14 ms
Maximum value of the facilitation variable y	y_{max}	NTF	1.32	1.32
Increment of the facilitation variable y	$y_{inc,1}$	NTF	0.39	0.39
Decay time constant of inactivation variable z	$1/ k_z$	NTF	3 s	3 s
Minimum value of the inactivation variable z	z_{min}	NTF	0.75	0.75
Decrement of the inactivation variable z	$z_{inc,1}$	NTF	0.4	0.4
Effective quantal size[6]	q^*		−6.6 pA	−6.6 pA

[1] Initial guesses for model parameter were derived from NTF decomposition analysis as indicated.
[2] Parameter values for the kinetic scheme with a MM-type saturation of the Ca^{2+} dependence the first priming step as illustrated in Fig. 1C1.
[3] Parameter values for the kinetic scheme with a linear Ca^{2+} dependence the first priming step but an additional empty and refractory release site state (ERS) as illustrated in Fig. 1C2.
[4] To optimally fit experimental data, $SP_{LS,rest}$ had to be increased by ~7% beyond the value predicted by NTF.
[5] Fractions s_1 and s_2 describe state transitions during low-frequency stimulation (f_{stim} = 5–20 Hz).
[6] This parameter takes into account the attenuation of eEPSCs peaks by 1 mM kyn and by the temporal dispersion of synchronous release (8, 9).

SI References

1. H. Taschenberger, A. Woehler, E. Neher, Superpriming of synaptic vesicles as a common basis for intersynapse variability and modulation of synaptic strength. *Proc Natl Acad Sci U S A* **113**, E4548-4557 (2016).
2. J. T. Ting, T. L. Daigle, Q. Chen, G. Feng, Acute brain slice methods for adult and aging animals: application of targeted patch clamp analysis and optogenetics. *Methods Mol Biol* **1183**, 221-242 (2014).
3. T. Wang, G. M. van Woerden, Y. Elgersma, J. G. G. Borst, Enhanced Transmission at the Calyx of Held Synapse in a Mouse Model for Angelman Syndrome. *Front Cell Neurosci* **11**, 418 (2017).
4. H. Taschenberger, R. M. Leao, K. C. Rowland, G. A. Spirou, H. von Gersdorff, Optimizing synaptic architecture and efficiency for high-frequency transmission. *Neuron* **36**, 1127-1143 (2002).
5. A. Y. Wong, B. P. Graham, B. Billups, I. D. Forsythe, Distinguishing between presynaptic and postsynaptic mechanisms of short-term depression during action potential trains. *J Neurosci* **23**, 4868-4877 (2003).
6. E. Neher, T. Sakaba, Combining deconvolution and noise analysis for the estimation of transmitter release rates at the calyx of Held. *J Neurosci* **21**, 444-461 (2001).
7. S. F. Traynelis, Software-based correction of single compartment series resistance errors. *J Neurosci Methods* **86**, 25-34 (1998).
8. E. Neher, H. Taschenberger, Non-negative Matrix Factorization as a Tool to Distinguish Between Synaptic Vesicles in Different Functional States. *Neuroscience* **458**, 182-202 (2021).
9. H. Taschenberger, V. Scheuss, E. Neher, Release kinetics, quantal parameters and their modulation during short-term depression at a developing synapse in the rat CNS. *J Physiol* **568**, 513-537 (2005).
10. E. Neher, Merits and Limitations of Vesicle Pool Models in View of Heterogeneous Populations of Synaptic Vesicles. *Neuron* **87**, 1131-1142 (2015).
11. N. Lipstein *et al.*, Munc13-1 is a Ca^{2+}-phospholipid-dependent vesicle priming hub that shapes synaptic short-term plasticity and enables sustained neurotransmission. *Neuron* **109**, 3980-4000 e3987 (2021).
12. X. Lou, V. Scheuss, R. Schneggenburger, Allosteric modulation of the presynaptic Ca^{2+} sensor for vesicle fusion. *Nature* **435**, 497-501 (2005).
13. H. von Gersdorff, R. Schneggenburger, S. Weis, E. Neher, Presynaptic depression at a calyx synapse: the small contribution of metabotropic glutamate receptors. *J Neurosci* **17**, 8137-8146 (1997).
14. R. Schneggenburger, E. Neher, Intracellular calcium dependence of transmitter release rates at a fast central synapse. *Nature* **406**, 889-893 (2000).
15. J. H. Bollmann, B. Sakmann, J. G. Borst, Calcium sensitivity of glutamate release in a calyx-type terminal. *Science* **289**, 953-957 (2000).
16. M. F. Cuttle, T. Tsujimoto, I. D. Forsythe, T. Takahashi, Facilitation of the presynaptic calcium current at an auditory synapse in rat brainstem. *J Physiol* **512**, 723-729 (1998).
17. J. G. Borst, B. Sakmann, Facilitation of presynaptic calcium currents in the rat brainstem. *J Physiol* **513**, 149-155 (1998).
18. F. Felmy, E. Neher, R. Schneggenburger, Probing the Intracellular Calcium Sensitivity of Transmitter Release during Synaptic Facilitation. *Neuron* **37**, 801-811 (2003).
19. M. Blatow, A. Caputi, N. Burnashev, H. Monyer, A. Rozov, Ca^{2+} buffer saturation underlies paired pulse facilitation in calbindin-D28k-containing terminals. *Neuron* **38**, 79-88 (2003).
20. N. P. Vyleta, P. Jonas, Loose coupling between Ca^{2+} channels and release sensors at a plastic hippocampal synapse. *Science* **343**, 665-670 (2014).
21. K. H. Lin, H. Taschenberger, E. Neher, Dynamics of volume-averaged intracellular Ca. *J Physiol* **595**, 3219-3236 (2017).
22. T. Sakaba, Roles of the fast-releasing and the slowly releasing vesicles in synaptic transmission at the calyx of held. *J Neurosci* **26**, 5863-5871 (2006).
23. T. Sakaba, E. Neher, Quantitative relationship between transmitter release and calcium current at the calyx of Held synapse. *J Neurosci* **21**, 462-476 (2001).